corresponds to an $\Omega = 1$, Friedmann zero-pressure universe, empty-beam angular diameter distances (corresponding to all the mass of the Universe concentrated in clumps outside the light beam[14,34]), $H_0 = 60\ \mathrm{km\ s^{-1}}$, and a lens at redshift $z_l = 0.3$ (near the minimum of $\sum_{cr}$ for source redshift $z_s = 1$). The dependence $A_s(z_l, z_s)$ is determined by d_{os} and $\sum_{cr}$. For the example of Fig. 2, for a source at $z_s = 1$ $d_{os} = 1{,}646$ Mpc and $\sum_{cr} = 0.69\ \mathrm{g\ cm^{-2}}$. For a source at $z_s = 2$, the values of d_{os}, $\sum_{cr}$ and A_s are modified by factors 1.14, 0.86 and 3.3, respectively.

To estimate the cluster surface mass densities consider an example of a rich and compact, approximately spherical and isothermal cluster with a line-of-sight velocity dispersion $\sigma_\parallel \sim 1500\ \mathrm{km\ s^{-1}}$, core radius 0.3 Mpc and redshift $z_l = 0.4$; a source at $z_s = 2$, and the universe as that considered in the example above. Then $\sum_{cr} = 0.57\ \mathrm{g\ cm^{-2}}$ and the central convergence is $\kappa_0 \sim 0.7$.

The properties of marginal lenses can explain some of the known observations and also they can allow us to search for this specific kind of lensing.

The dominance of subcritical lensing for superclusters may explain the failure to find alignment of extended radio sources[23,24]. The area A_s may be $\sim$arc s^2, whereas the image separations are of the order of many arc seconds. Under such circumstances there cannot be any alignment on the scale of arc degrees sought by refs 23 and 24. Faint radio sources for which a shape can be resolved by modern techniques are separated by more then 10′ on average[25]. Such a source must fall within the caustic to be multiply imaged. Therefore, even if sampling on the scale of arc minutes were attempted, the statistical effect on alignment would be very small.

The most promising means to seek gravitational lensing by superclusters seems at present to be looking for multiply imaged objects in the fields of 'quasar clusters'.

Recently, a gravitational lens candidate pair of quasar images, Q1146+111 B, C, of very large separation was reported[26] on the basis of striking similarities of their spectra. Later, differences in emission lines were found[27,35], though it could be argued that the differences could be due to arrival time differences (which are $\sim 10^3$ years and can allow for variations in a volume of linear size $\sim$1 kpc). The probablity of a chance coincidence must be smaller than that calculated by ref. 28, because they did not take into account the known and unusual spectral similarities. In any case the pair Q1146+111 B,C requires further investigation before it can be determined whether they are separate quasars or two images of the same quasar.

A way to distinguish between these possibilities (suggested by B. Paczyński) is to look at galaxies at the redshift of the quasar pair in the immediate area of the pair. If the pair is produced by marginal lensing, some of the galaxies may be unusually large for their redshift, whereas some may be actually crossed by the lens caustics and have unusual lopsided shapes[5].

Regardless of the fate of Q1146+111 B,C, this pair may be either a representative or a prototype of groups of quasar images with similar properties still to be discovered. Taking it as the latter, it is interesting to note that the pair exhibits the properties of marginal lensing: there is no prominent concentration of galaxies in the area of the pair, there is the 'quasar cluster'[29], there are unsplit images of quasars with larger redshifts close to the pair on the scale of image separation, and the microwave inhomogeneity was not detected on the angular scale of image separation[22] though it should be detectable for standard-type lens models[7,22,30,31].

There are a few known 'quasar clusters'[29] and groups of quasar images of close redshift and separations of the order of arc minutes[32]. Some of them may be the result of gravitational lensing by superclusters. An investigation of these areas of the sky by currently available techniques (for example, ref. 33 and J. E. Gunn, personal communication) could reveal multiple images of galaxies as well as quasars, which could yield information on supercluster structures and masses.

I thank Y. Avni, J. H. van Gorkom, J. R. Gott, J. E. Gunn, A. J. S. Hamilton, A. Kashlinski, C. G. Lacey, T. R. Lauer, M. Milgrom, J. P. Ostriker, B. Paczyński, H. J. Rood, E. L. Turner and D. Weinberg for helpful advice, comments, conversations, discussions and remarks. The work was supported by the Dr Chaim Weizmann postdoctoral fellowship of the Princeton University and by Stiftung Volkswagenwerk at the Weizmann Institute.

Received 7 July; accepted 30 October 1986.

1. Sanders, R. H., van Albada, T. S. & Oosterloo, T. O. *Astrophys. J.* **278,** L91-L94 (1984).
2. Narayan, R., Blandford, R. & Nitiyananda, R. *Nature* **310,** 112-115 (1984).
3. Turner, E. L., Ostriker, J. R. & Gott, J. R. *Astrophys. J.* **284,** 1-22 (1984).
4. Subramanian, K. & Cowling, S. A. *Mon. Not. R. astr. Soc.* **219,** 333-346 (1986).
5. Kovner, I. *Astrophys. J.* (in the press).
6. Sarazin, C. L. *Rev. mod. Phys.* **58,** 1-115 (1986).
7. Ostriker, J. P. & Vishniac, E. T. *Nature* **322,** 804 (1986).
8. Oort, J. H. *A. Rev. Astr. Astrophys.* **21,** 373-428 (1983).
9. Efstathiou, G. & Silk, J. *Fundam. Cosmic Phys.* **9,** 1-138 (1983).
10. Jaroszyński, M. & Paczyński, B. in *Proc. Second Eur. Reg. Mg (IAU) (Memorie Soc. astr. ital.* **45**) 673-480 (1974).
11. Schneider, P. *Astr. Astrophys.* **143,** 413-420 (1984).
12. Blandford, R. & Narayan, R. *Astrophys. J.* **310,** 568-582 (1986).
13. Kovner, I. *Astrophys. J.* (in the press).
14. Kovner, I. *Astrophys. J.* (in the press).
15. Struble, M. F. & Rood, H. J. *Astr. J.* **87,** 7-46 (1982).
16. de Lapparent, V., Geller, M. J. & Huchra, J. P. *Astrophys. J.* **302,** L1-L5 (1986).
17. Tago, E., Einasto, J. & Saar, E. *Mon. Not. R. astr. Soc.* **218,** 177-184 (1986).
18. Arnold, V. I., Shandarin, S. F. & Zel'dovich, Ya. B. *Geophys. Astrophys. Fluid Dyn.* **20,** 111-130 (1982).
19. Vishniac, E. T., Ostriker, J. P. & Bertschinger, E. *Astrophys. J.* **291,** 399-416 (1985).
20. Bourassa, R. R., Kantowski, R. & Norton, T. D. *Astrophys. J.* **185,** 747-756 (1973).
21. Kaiser, N. & Stebbins, A. *Nature* **310,** 391-393 (1984).
22. Stark, A. A., Dragovan, M., Wilson, R. W. & Gott, J. R. *Nature* **322,** 805 (1986).
23. Sanders, R. H. *Nature* **309,** 35-37 (1984).
24. Kapahi, V. K., Subramanyan, R. & Singal, A. K. *Nature* **313,** 463-465 (1984).
25. Windhorst, R. thesis, Univ. Leiden (1984).
26. Turner, E. L. *et al. Nature* **321,** 142-144 (1986).
27. Shaver, P. A. & Cristiani, S. *Nature* **321,** 585-586 (1986).
28. Phinney, E. S. & Blandford, R. D. *Nature* **321,** 570-571 (1986).
29. Arp, H. & Hazard, C. *Astrophys. J.* **240,** 726-736 (1980).
30. Paczyński, B. *Nature* **321,** 419-420 (1986).
31. Gott, J. R. *Nature* **321,** 420-421 (1986).
32. Paczyński, B. *Nature* **319,** 567-568 (1986).
33. Tyson, J. A., Valdes, F., Jarvis, J. F. & Mills, A. P. *Astrophys. J.* **281,** L59-L62 (1984).
34. Dyer, C. C. & Roeder, R. C. *Astrophys. J.* **174,** L115-L117 (1972).
35. Huchra, J. P. *Nature* **323,** 784-786 (1986).

Morphology of the geomagnetic field and implications for the geodynamo

David Gubbins*‡ & Jeremy Bloxham†

* Bullard Laboratories, Cambridge University, Cambridge CB3 0EZ, UK
† Department of Earth and Planetary Sciences, Harvard University, Cambridge, Massachusetts 02138, USA

Maps of the radial component of the magnetic field at the surface of Earth's core for 1715–1980 show, on average, a pattern of four lobes, placed symmetrically about the Equator, and zero flux near the poles. Time variations are largely confined to the Atlantic hemisphere (90° E to 90° W). We propose this average field to be the true dynamo-generated field; that equatorial symmetry is a fundamental consequence of the dynamo equations; and that the polar patches are because of the dynamical influence of the inner core. The main lobes are 120° apart and we propose that the flux from a missing third pair of lobes, which should appear symmetrically near the Greenwich meridian, has been re-distributed by near-surface fluid flow to generate secular variation in the Atlantic hemisphere.

New methods, based on inverse theory, of analysing magnetic measurements[1,2] have yielded maps of the magnetic field at the

‡ Present address: Research School of Earth Sciences, Australian National University, Canberra, ACT 2601, Australia.

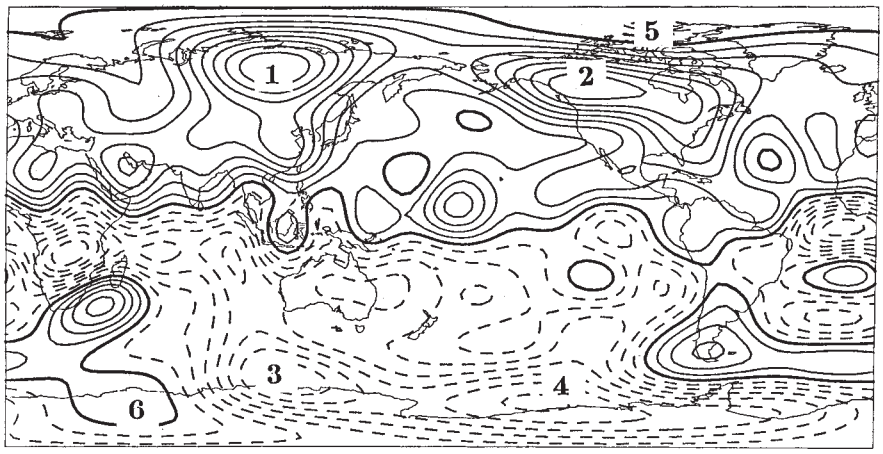

Fig. 1 Map of the radial component of the magnetic field at the core-mantle boundary for 1980 (ref. 3). Contour interval is 100 μT; solid contours represent flux into the core, broken contours flux out of the core; bold contours represent zero radial field. The two main pairs of lobes (1,3) and (2,4) are indicated, as are the patches of low radial field (5 and 6) near the poles.

Fig. 2 As Fig. 1 but viewed from the North Pole in a Lambert azimuthal equal-area projection. The projection of the inner core onto the core-mantle boundary is described by the bold circle centred on the North Pole.

core-mantle boundary (CMB) with greatly improved resolution and accuracy[3–5]. The fields are displayed by their radial component; a map for 1980, based on data from the Magsat satellite, assuming an insulating mantle, is shown in Fig. 1. The earliest map draws on data from AD 1695[5,6] (ref. 5 and J.B. and D.G., in preparation). We can track movement of radial features by comparing maps at different epochs. Drifting features, which almost invariably move westwards, have been confined to the Atlantic hemisphere for the entire period—long enough to show features forming and disappearing at the edges of the region. The observation of low secular variation at the CMB beneath the Pacific should be distinguished from the well-known observations of low secular variation in this region at the Earth's surface based on palaeomagnetic measurements[6].

Some features are stationary. By far the most striking of these are the four concentrations of flux (lobes) marked 1–4 in Fig. 1. With a typical westward drift rate of 0.2° yr^{-1} we would expect these features to have drifted by over 50° in longitude during this period: such a large drift would be clearly detectable and has most certainly not occurred. The lobe beneath Canada appeared to split in the nineteenth century, possibly owing to an interaction with a moving feature (J.B. and D.G., in preparation). Low polar flux is another persistent feature (marked 5, 6 in Fig. 1). The North-Pole patch is consistent between epochs, the southern one less so—it is displaced some distance from the pole in 1980, perhaps because the patch of negative flux beneath South America has displaced it and lobe 3 (J.B. and D.G., in preparation).

We ignore all drifting features and the smaller static ones, like that in the central Pacific: there remains an average field (AF) consisting of four main lobes and zero flux near the poles. At the Earth's surface it is predominantly dipolar, but otherwise quite dissimilar from the present-day field. It has two remarkable properties: antisymmetry about the Equator (pairs of lobes lie on the same longitude, near 120° E and 120° W), and zero intensity near the poles (where a dipole field would achieve maxima). Equatorial antisymmetry requires that $\{g_l^m, h_l^m\} = 0$ if $l-m$ is even, in terms of standard geomagnetic coefficients[7].

We postulate that AF is the main standing field generated by the dynamo. The SV may partake in the generation process (as in a MAC-wave dynamo[8], for example), or it may simply be a consequence of near surface motions unrelated to dynamo action.

Dyamo-generated fields allowed the observed hemispheric symmetry. Solutions to the equations governing incompressible flow driven by buoyancy (thermal or compositional), Coriolis, and magnetic forces may satisfy[9,10]

$$P(\pi-\theta) = -P(\theta)$$
$$T(\pi-\theta) = T(\theta)$$
$$p(\pi-\theta) = p(\theta)$$
$$t(\pi-\theta) = -t(\theta)$$
$$S(\pi-\theta) = S(\theta)$$

where θ is a colatitude, S is temperature (or composition), $\mathbf{u}$ velocity, and $\mathbf{B}$ magnetic field with

$$\mathbf{u} = \nabla \wedge t\hat{\mathbf{r}} + \nabla \wedge \nabla \wedge p\hat{\mathbf{r}}$$
$$\mathbf{B} = \nabla \wedge T\hat{\mathbf{r}} + \nabla \wedge \nabla \wedge P\hat{\mathbf{r}}$$

The opposite symmetry is not allowed. Hemispheric symmetry has been used in spherical convection and dynamo calculations to speed computation[9,10]. The hemispheric solution is believed more unstable, and therefore more physically realisable.

The dynamics of the core are dominated by Coriolis forces, the boundaries, and possibly magnetic forces associated with large toroidal field. In the regions above and below the inner core the boundaries are roughly perpendicular to the rotation axis: these regions resemble plane layers. In equatorial regions the boundaries are roughly parallel to the rotation axis, resembling the geometry of a cylindrical annulus rotating about its axis. Both these geometries have been studied extensively and

exhibit quite different dynamical behaviour[11]; accordingly, we expect the behaviour inside the projection of the inner core, along the rotation axis, onto the CMB, which is a circle of 20.4° (Fig. 2), to be different from that outside. The positions of the two main lobes in each hemisphere are consistent with convection rolls parallel to the rotation axis and tangential to the inner core. In Busse's simple model[12] each convection roll has flow along its length induced by the boundary providing the helicity required for dynamo action. Downwelling flow along the rolls will concentrate flux as observed; alternating with these rolls we expect other rolls along which the flow is towards the CMB. Such a roll should be centred on 180° (midway between the concentrations of flux at 120° E and 120° W), where we observe low flux as a result of the upwelling.

The location of the main lobes near 120° W and 120° E suggests a missing third pair of lobes near Greenwich meridian resulting in a three-fold azimuthal symmetry. This would result from a total of six convection rolls, three with flow away from the CMB, and three with flow towards the CMB. The 'missing' third pair of lobes would be in the Atlantic Ocean where the secular variation is strong. We propose that the vigorous fluid motions associated with this stronger secular variation have prevented their formation.

The inner core circle is comparable in size with the zero flux patch observed there (Fig. 2); this may be a result of the different dynamics in this region.

We have presented a highly idealized model of the geodynamo, for a spherical symmetric Earth, with a three-fold azimuthal symmetry and perfect antisymmetry about the equator. In a companion paper we argue that this simple picture is complicated by the effect of lateral heterogeneities in the lower mantle on the flow in the core, which may explain the asymmetrical nature of the secular variation and control the azimuthal orientation of the rolls and other features.

This work was supported by NERC grant GR3-3475 and NSF grants EAR-8317594 and EAR-8608890.

Received 9 July; accepted 13 November 1986.

1. Shure, L., Parker, R. L. & Backus, G. *Phys. Earth planet. Inter.* **28**, 215–229 (1982).
2. Gubbins, D. *Geophys. J. R. astr. Soc.* **73**, 641–652 (1983).
3. Gubbins, D. & Bloxham, J. *Geophys. J. R. astr. Soc.* **80**, 695–713 (1985).
4. Shure, L., Parker, R. L. & Langel, R. A. *J. geophys. Res.* **90**, 11505–11512 (1985).
5. Bloxham, J. & Gubbins, D. *Nature* **317**, 777–781 (1985).
6. Doell, R. R. & Cox, A. *Science* **171**, 248–254 (1971).
7. Chapman, S. & Bartels, J. *Geomagnetism* (Oxford University Press, 1962).
8. Braginsky, S. I. *Sov. Phys. JETP* **20**, 1462–1471 (1965).
9. Young, R. E. *J. Fluid Mech.* **63**, 695–721 (1974).
10. Gubbins, D. *Geophys. J. R. astr. Soc.* **42**, 295–305 (1975).
11. Chandrasekhar, S. *Hydrodynamic and Hydromagnetic Stability* (Oxford University Press, 1961).
12. Busse, F. H. *Geophys. J. R. astr. Soc.* **42**, 437–460 (1975).

Thermal core–mantle interactions

Jeremy Bloxham* & David Gubbins†‡

* Department of Earth and Planetary Sciences, Harvard University, Cambridge, Massachusetts 02138, USA
† Bullard Laboratories, Cambridge University, Cambridge CB3 0EZ, UK

Maps of the magnetic field at the core–mantle boundary for 1715–1980 reveal static features in the field and an absence of westward drift from much of the core–mantle boundary. The static features suggest that flow in the core is coupled to the mantle. We examine different coupling mechanisms and predict lateral inhomogeneity at the core–mantle boundary. Comparison with models of the lower mantle and core–mantle boundary derived seismically and from the geoid is encouraging, though their resolution is currently inadequate for a full comparison to be made with the much better-resolved magnetic field.

In an earlier paper[1] we presented models of the magnetic field at the core-mantle boundary (CMB) at approximately 60 yr intervals from 1715 to 1980. We showed that the secular variation (SV) is confined mainly to the hemisphere 90° E to 90° W, where its character has remained unaltered throughout the 265 yr timespan of the models. Elsewhere we identified static features in the field at the CMB. We suggested that this confinement of SV to one hemisphere and the presence of many static features is the result of coupling of flow in the core to the mantle. Mean zonal flows are expected on theoretical grounds[2,3]: the absence of westward drift of features in the field at the CMB in the Pacific hemisphere suggests that flow in the core may be coupled to the mantle. The flux patches beneath Siberia and Canada, which we have identified with convection rolls[4], should also drift[5]: no drift of these features is observed.

Stationary patches of intense field (static flux bundles) are labelled 1–5 in Fig. 1; they were attributed to flux concentration by downwelling fluid, associated with cold mantle, balancing diffusive decay[1]. Likewise, upwelling may form zero flux patches (labelled 6–9 in Fig. 1) by sweeping field lines away, although we believe the polar patches (6 and 9) to be associated with the

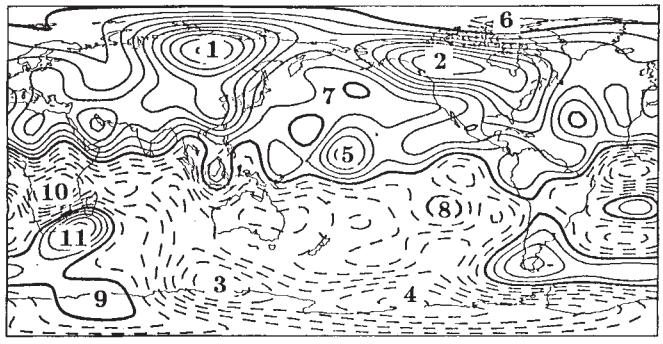

Fig. 1 Map of the radial component of the magnetic field at the core-mantle boundary for 1980 (ref. 6), produced assuming an insulating mantle. Contour interval is 100 μT; solid contours represent flux into the core, broken contours flux out of the core; bold contours represent zero radial field. The following features are indicated: static flux bundles (1–5); static zero flux patches (6–9); core spots (10–11).

dynamical influence of the inner core[4]. In regions where the subsurface toroidal field is strong, upwelling will concentrate intense field beneath the CMB[7,8] leading to the formation of core spots. The core spot pair (10–11) appeared to form under the western Indian Ocean and intensified beneath southern Africa.

We propose that flow in the core is thermally coupled to the lower mantle, with upwelling beneath hot regions of the lower mantle and downwelling beneath cold regions. Such an argument may be too simplistic: the problem of coupled convection between two fluids of such vastly different properties requires careful analysis. Jones[9] has argued that lateral temperature variations on the CMB will only affect the flow in a thin layer near the CMB. If the upper regions of the core are strongly stably stratified then such effects will be confined to a thin layer, but if we assume the whole core convects then lateral temperature variations in the lowermost mantle may affect a larger region. Free convection in the core, resulting most probably from crystallization at the inner core boundary, drives the dynamo. Free convection is driven in the lower mantle, in large part, by the heat flux from the core. Convection in the lower mantle results in large lateral temperature variations just above

‡ Present address: Research School of Earth Sciences, Australian National University, Camberra, ACT 2601, Australia.